Birth Defects Research

WILEY

Birth Defects Research | Society for Birth Defects Research & Prevention

RESEARCH ARTICLE OPEN ACCESS

Examining the Neurodevelopmental Impact of Sonic Hedgehog Pathway Inhibition in Mice

Tyler G. Beames[1] | Megan Y. Stewart[1] | Rachel B. Walkup[1] | Jules B. Panksepp[2] | Robert J. Lipinski[1]

[1]Department of Comparative Biosciences, School of Veterinary Medicine, University of Wisconsin-Madison, Madison, Wisconsin, USA | [2]Waisman Center, University of Wisconsin-Madison, Madison, Wisconsin, USA

Correspondence: Robert J. Lipinski (robert.lipinski@wisc.edu)

Received: 22 November 2024 | **Revised:** 13 March 2025 | **Accepted:** 17 March 2025

Funding: This work was supported by the National Institute of Child Health and Human Development; National Institutes of Health under awards R01ES026819, F31ES034632, P50HD105353, and T32ES007015; National Institute of Environmental Health Sciences; University of Wisconsin-Madison.

Keywords: behavioral assay | craniofacial morphogenesis | neurodevelopmental disorder | sonic hedgehog signaling

ABSTRACT

Background: Neurodevelopmental disorders (NDDs) are common, highly variable, and etiologically complex. Identifying environmental factors that adversely impact prenatal brain development is a direct path to NDD prevention. Small molecule disruption of the Sonic hedgehog (Shh) signaling pathway, a key regulator of craniofacial morphogenesis, can lead to overt face and forebrain malformations that produce profound neurological deficits. However, whether environmental disruption of Shh signaling can cause subtle neurodevelopmental outcomes in the absence of overt facial malformations was unknown.

Methods: We developed a dietary model of Shh signaling inhibition using the specific Shh pathway antagonist vismodegib. C57BL/6J mice were fed control chow or chow containing 25, 75, or 225 ppm vismodegib from gestational day (GD)4 through GD12 to target Shh signaling during craniofacial morphogenesis. Impacts of Shh pathway disruption on face and forebrain development were examined in exposed embryos and fetuses, and behavioral characteristics were assessed in adult mice.

Results: Exposure to chow containing 225 ppm vismodegib resulted in abnormal forebrain patterning at GD11, face and brain malformations at GD17, and early postnatal mortality, while lower treatment groups appeared phenotypically normal. Adult mice exposed to 25 and 75 ppm vismodegib outperformed control mice on repeated rotarod sessions, but treated mice did not significantly differ from control animals in open field exploration, marble burying, olfactory discrimination and detection, or fear conditioning assays.

Conclusions: Under the examined conditions, prenatal Shh disruption did not produce robust neurobehavioral differences in the absence of craniofacial malformations.

1 | Introduction

As increased awareness and improved diagnostic criteria have revealed higher incidences of neurodevelopmental disorders (NDDs) such as autism, attention-deficit/hyperactivity disorder, and intellectual disabilities, efforts to prevent these conditions have met with substantial challenges. A growing body of epidemiological and experimental evidence underscores the role of the environment in NDD occurrence, and reducing exposure to environmental toxicants remains the most effective path to prevention (De Felice et al. 2015; Lan et al. 2017; Lyall et al. 2017; Wagner et al. 2006). However, identifying individual risk factors is complicated by the etiologically complex nature of most common NDDs. Moreover, it is not feasible to assess the neurobehavioral impacts of all chemicals and mixtures that make up the exposome. Focusing instead on elucidating environmentally

sensitive signaling pathways that contribute to NDDs presents a more direct approach to characterizing risk based on common mechanisms of toxicity.

The Sonic hedgehog (Shh) signaling pathway is a key regulator of craniofacial morphogenesis that is sensitive to both genetic and environmental perturbation (Chen 2016; Everson et al. 2019; Roessler et al. 1996; Solomon et al. 2012). During embryogenesis, this paracrine factor plays a role in early neurospecification, promoting a ventral identity along the length of the neural tube and within the developing forebrain by counterbalancing dorsalizing factors such as BMPs and Wnt ligands (Ericson et al. 1995; Furuta et al. 1997; Roelink et al. 1995). Shh is also required for the development of the medial ganglionic eminence (MGE), a transient forebrain structure that gives rise to GABAergic cortical interneurons (Butt et al. 2005; Fuccillo et al. 2004; Wichterle et al. 2001; Xu et al. 2004), as well as for the expansion of the ventromedial forebrain (Britto et al. 2002; Chiang et al. 1996). In addition to its role in forebrain morphogenesis, Shh drives the growth of the cranial neural crest-derived mesenchyme that gives rise to the connective tissue of the face (Jeong et al. 2004).

Disruption of the Shh pathway by both genetic and environmental factors causes craniofacial malformations including holoprosencephaly (HPE), a condition defined by medial forebrain deficiency and commonly co-occurring with midfacial dysmorphology (Addissie et al. 2021; Chiang et al. 1996; Dubourg et al. 2018; Everson et al. 2019; Richieri-Costa and Ribeiro 2010; Solomon et al. 2012). While severe (i.e., alobar) HPE is rarely compatible with postnatal survival, moderately affected individuals may survive with significant cognitive impairments, and individuals with microform HPE can appear phenotypically normal (Tekendo-Ngongang et al. 2020). This variability in individuals with HPE supports a multifactorial model of pathogenesis in which environmental factors act together or in concert with genetic predispositions to modulate disease severity (Addissie et al. 2021; Everson et al. 2019; Hong and Krauss 2012, 2018; Petryk et al. 2015). Moreover, the inherent sensitivity of Shh signaling to small molecule disruption highlights the potential for environmental Shh pathway antagonists to contribute to HPE incidence and severity. Recently, a study in mice demonstrated that chemical disruption of Shh can alter brain development at doses that cause only subtle craniofacial dysmorphology (Everson et al. 2019). This observation supports a model of environmental Shh pathway inhibition in which neurological function is altered in the absence of overt structural malformations.

To test the hypothesis that Shh signaling-mediated neurobehavioral deficits can be induced in mice without causing overt facial dysmorphology, we developed a dietary model of Shh pathway inhibition. As a surrogate for the dozens of small molecule pathway inhibitors that have been described, pregnant mice were exposed to the potent and specific Shh pathway inhibitor vismodegib throughout the critical window for HPE. After determining an overtly teratogenic dose based on craniofacial morphology, lower doses were assessed for impacts on early forebrain patterning, face and brain morphology later in development, and behavior in adult mice.

2 | Materials and Methods

2.1 | Materials

Vismodegib (Catalog No. V-4050; LC Labs) used in diet formulation was manually pulverized to achieve a uniform powder and suspended in soybean oil (Catalog N. S0255; Spectrum Chemical Mfg. Corp) prior to inclusion in rodent chow pellets.

2.2 | Animals

Animal studies were conducted in strict accordance with the recommendations in the *Guide for the Care and Use of Laboratory Animals* of the National Institutes of Health. Studies followed procedures approved by the Institutional Animal Care and Use Committees of the University of Wisconsin School of Veterinary Medicine (protocol V005396) and Letters and Sciences and Vice Chancellor for Research Centers (protocol G005373). C57BL/6J mice (Strain No. 00664, Jackson Laboratories) were housed in rooms maintained at 22°C ± 2°C and 30% to 70% humidity on a 12 h light, 12 h dark cycle. Mice were fed Irradiated Soy Protein-Free Extruded Rodent Diet (Catalog No. 2920x; Envigo Teklad Global) until a copulation plug was detected, at which point dams received Irradiated Teklad Global 19% Protein Extruded Rodent Diet (breeder chow, Catalog No. 2919; Envigo Teklad Global) except when on experimental diets. Dams were euthanized via carbon dioxide asphyxiation followed by cervical dislocation at GD11 for embryo collection, GD17 for fetal collection, and after weaning for behavioral studies.

2.3 | Dietary Exposure Procedure

Precision timed-matings were achieved by placing one to two nulliparous C57BL/6J wild-type female mice with a single C57BL/6J male mouse for 1–2 h (Heyne, Plisch, et al. 2015). Following the mating period, females were examined for the presence of a copulation plug, and the initiation of the mating period was designated as gestational day (GD)0. Vismodegib suspended in soybean oil was used to generate vismodegib-containing diets that were prepared from Envigo base diet (Catalog No. 2919; Envigo Teklad). Control chow diet was prepared with soybean oil alone. Control and vismodegib treatment diets were introduced to pregnant female mice at GD4. Dams were placed back on standard breeder chow at GD12.

2.4 | Facial Morphometrics and Fetal Brain Morphology

Pregnant dams were administered control chow or 25, 75, or 225 ppm vismodegib chow from GD4 through GD12. Following euthanasia at GD17, uterine horns were dissected. Resorptions, live fetuses, and crown-rump length were recorded, and gross morphological abnormalities were noted. For facial morphometric analyses, fetuses were fixed in 10% phosphate buffered formalin for at least 1 week before being imaged by light microscopy. To ensure the reliability of image-based measurements, consistent head and face orientation were maintained across all images. Light microscopic images were captured using an

Olympus QImaging MicroPublisher 5.0 camera (QImaging) connected to an SZX-10 stereomicroscope (Olympus). ImageJ software was used to quantify interocular distance (IOD) and upper lip length (ULL) from facial images as previously described (Everson et al. 2019). All measurements were taken by a single rater.

For qualitative assessment of correlative face and brain morphology, fetuses were fixed in Bouin's solution for at least 1 week before being imaged for facial morphology. Bouin's-fixed brains were then dissected out and imaged dorsally. Brains were washed in 70% ethanol until the ethanol ran clear before being paraffinized and paraffin-embedded for sectioning. Coronal sections through the cerebrum were stained using hematoxylin and eosin (H&E) prior to imaging. Light microscopic images of fetal faces, whole brains, and H&E-stained sections were captured using an Olympus QImaging MicroPublisher 5.0 camera connected to an SZX-10 stereomicroscope.

2.5 | In Situ Hybridization

Following euthanasia of dams and uterine dissection at GD11, embryos were dehydrated in graded solutions of methanol until staining. In situ hybridization was performed using a high-throughput technique which allowed samples to be identically processed across treatment groups (Abler et al. 2011). Embryos were hemisected mid-sagittally prior to staining. Embryos were then incubated in proteinase K (10 μg/mL) with collagenase (1 mg/mL) for 2 min before initial washes. The primer sequences used for probe generation include a T7-polymerase recognition site and a 5-bp leader sequence on the reverse probe. RNA probe sequences, with recognition site and leader underlined, are as follows: *Gli1* [forward-CCCTCCTCCTCTCATTCCAC and reverse-CGATGTTAATACGACTCACTATAGGGTCCAGCTGAGTGTTGTCCAG], *Pax6* [forward- AGTGAATGGGCGGAGTTATG and reverse- CGATGTTAATACGACTCACTATAGGGAGTGTGTGTTGTCCCAGGTTC], and *Nkx2-1* [forward-CCGCAAAGACCACCATTC and reverse-CGATGTTAATACGACTCACTATAGGGGGGTTATGCTGAAGACTTTCC].

Following staining, embryos were imaged by light microscopy using a QImaging MicroPublisher 6 camera connected to an Olympus SZX-10 stereomicroscope. Area measurements of the MGEs and head were made in ImageJ. Measurements were made by a single rater blinded to the treatment group.

2.6 | Behavioral Assays

For behavioral testing, litters from vehicle- and vismodegib-treated dams were weaned at 3 weeks of age, and males and females were placed in separate home cages. Mice were selected for behavioral testing at random, and no more than three males and three females were chosen from a single litter for an average of 2 mice of each sex per litter per treatment group. Eight- to ten-week-old mice were transferred to the Waisman Center Behavioral Testing Service and given 1 week to acclimate. Assays were conducted in the order listed below, beginning with the least stressful test and finishing with the most stressful. Mice were placed on a cart and transported to the respective testing rooms for 30 min to acclimate before the start of each assay.

2.6.1 | Open Field

Mice were placed in an arena (43 cm^3) and allowed to move freely through the environment for 30 min. A 16 × 16 photobeam array surrounding each arena was used to monitor the position, horizontal locomotion, vertical activity, and stereotypic movement of each mouse during the testing period using Fusion 6.5 SuperFlex software. Position was defined as the center of the mouse, and the proportion of time the mouse spent in the center (internal 25% floor area) versus the periphery (external 75% floor area) of the chamber was determined.

2.6.2 | Marble Burying

Twenty marbles were arranged in 4 rows (5 marbles/row) within a standard home cage (20 × 32 cm) containing fresh bedding at a depth of 4 cm. Mice were individually placed in the test cage covered with a top for 30 min. At the end of the testing period, mice were returned to their home cages, and the number of marbles buried was counted. Marbles were considered buried only if they were 100% covered by bedding.

2.6.3 | Rotarod

Mice were placed on rotating drums of an accelerating rotarod (Med Associates Inc.) to evaluate motor coordination and balance. Rota-Rod 2 computer software was used. Over the course of the assay, the rotarod accelerated continuously from 4 to 40 rpm over a 5 min period. Each mouse received 4 trials with ~20 min between each trial. Latency to fall and rotation speed upon falling were recorded. For mice that remained on the rotarod for the duration of the test, the maximum possible latency (300 s) is reported.

2.6.4 | Olfactory Discrimination and Detection

The olfactory discrimination assay consisted of two sessions. In the first session, two cotton-tipped swabs (Dukal) were inserted into the home cage through a Plexiglas cover. The swabs were equally spaced from the walls of the cage and each other, with each swab tip located ~8 cm above the bedding. One swab was dampened with 2 μL water (familiar scent) and the other with 2 μL of either lemon or mint extract (both novel scents). The use of lemon or mint as the novel scent, as well as their placement in the cages, was pseudo-randomized and counter-balanced across groups. Time spent investigating each swab was recorded over a 3-min period, followed by a 3-min rest period. For the second session, the mice were provided one swab with mint extract and one swab with lemon extract. Placement of each swab was randomized. In this session, each mouse had access to a familiar scent and a novel scent. Time spent investigating each swab was again recorded for 3 min.

TABLE 1 | Litter statistics for fetuses at GD17.

Treatment	Litters collected [*n*]	Live fetuses [*n* (mean)]	Resorptions [*n* (mean)]	Crown-rump [mean ± SD mm]
Vehicle	7	47 (6.7)	9 (1.3)	17.23 ± 0.95
25 ppm Vis.	8	49 (6.1)	12 (1.5)	16.92 ± 1.12
75 ppm Vis.	8	55 (6.9)	14 (1.8)	16.95 ± 0.81
225 ppm Vis.	8	36 (4.5)*	22 (2.8)*	16.74 ± 0.79

*$p < 0.05$.

To assess olfactory detection, mice were first familiarized with a novel food item (TestDiet, LabTab, Sucrose Choc, 45 mg pellet, ~10 pellets per mouse) in their home cage. Next, mice were housed singly and deprived of food for 24 h. Testing commenced once a single food pellet was buried in a corner of the home cage at a depth of 1 cm below the bedding. Mice were given 5 min to explore the cage, and the latency to find the buried food was recorded.

2.6.5 | Fear Conditioning

Fear conditioning tests consisted of one training session and two testing sessions, and freezing was measured throughout each session. ANY-maze software (v4.1) was used to monitor freezing and control stimulus delivery. For training, a single mouse was placed in a fear conditioning chamber (Ugo Basile) cleaned with 70% ethanol. After a 120 s acclimation period, mice were exposed to a 30 s, 87 dB noise cue (conditioned stimulus, CS). During the last 2 s of the cue presentation, mice were delivered a scrambled, 0.7 mA shock (unconditioned stimulus, US) from the floor of the test cage. After 120 s, mice were exposed to another 30 s, 87 dB white noise cue co-terminating with a 0.7 mA shock. Mice were monitored for an additional 60 s after the second CS-US pairing before being returned to their home cages.

Twenty-two hours post-training, mice were placed back in the 70% ethanol-cleaned chambers for contextual fear recall testing. Freezing was again measured as mice explored the chamber for 360 s in the absence of an auditory cue or shock delivery. Mice were then returned to their home cages for 2 h. For cued fear recall testing, mice were placed in the fear conditioning chamber, now altered with gray plastic floor panels covering the shock grid, checkered wall inserts, and cleaned with 30% isopropyl alcohol instead of 70% ethanol. Mice were introduced to this altered context for a 120 s acclimation period before being exposed to the 30 s CS only. Mice were then able to free-roam for 120 s before another CS event. Mice remained in test cages for an additional 60 s before being returned to their home cages.

2.7 | Statistical Analysis

Statistical analyses were performed using GraphPad Prism 9 for morphometric assessments and MGE size. One-way ANOVA with Tukey's post hoc test was used to analyze IOD and ULL in GD17 mice and MGE area in GD11 mice. Behavioral endpoints were analyzed in R (Version 4.4.0). Normality of the data was assessed using Shapiro–Wilk test. Normal and log-normal data were evaluated for treatment- and sex-dependent effects using two-way ANOVA and Tukey's post hoc test. Data that failed normality testing were analyzed using aligned-rank transform ANOVA with post hoc test for multiple comparisons (Elkin et al. 2021; Wobbrock et al. 2011). An alpha value of 0.05 was maintained for the determination of statistical significance.

3 | Results

3.1 | Dose-Dependent Impacts of Shh Inhibition on Face and Brain Morphogenesis

Vismodegib, a therapeutic drug designed to treat Shh-active cancers, was previously shown to inhibit the Shh pathway in vitro and cause a variety of craniofacial and limb defects following an acute prenatal dose in animal models (Heyne, Melberg, et al. 2015; Robarge et al. 2009). A pilot study demonstrated that prenatal exposure to a diet of 225 ppm vismodegib induced robust craniofacial malformations consistent with Shh pathway inhibition. In the present study, two lower-dose diets separated by three-fold intervals (i.e., 25 and 75 ppm) were included with the goal of achieving exposures that did not produce overt dysmorphology.

Pregnant mice were provided vehicle- or vismodegib-containing chow between GD4 and GD12 to encompass key critical periods of Shh-mediated craniofacial morphogenesis. No significant differences in chow consumption were observed between treatment groups from GD4 to GD12 (Figure S1). For fetal endpoints, dams were euthanized at GD17, and litters were assessed for live fetuses, resorptions, and crown-rump length. Fetuses were fixed in formalin for facial morphometric analysis or Bouin's solution for assessment of brain phenotypes. Relative to vehicle-treated litters, there were fewer live fetuses and more resorptions following exposure to 225 ppm vismodegib, though crown-rump length in live fetuses was not significantly impacted by treatment (Table 1).

3.1.1 | Impacts on Craniofacial Morphogenesis

Previous mouse models of HPE demonstrate that IOD and ULL are sensitive predictors of underlying changes in brain

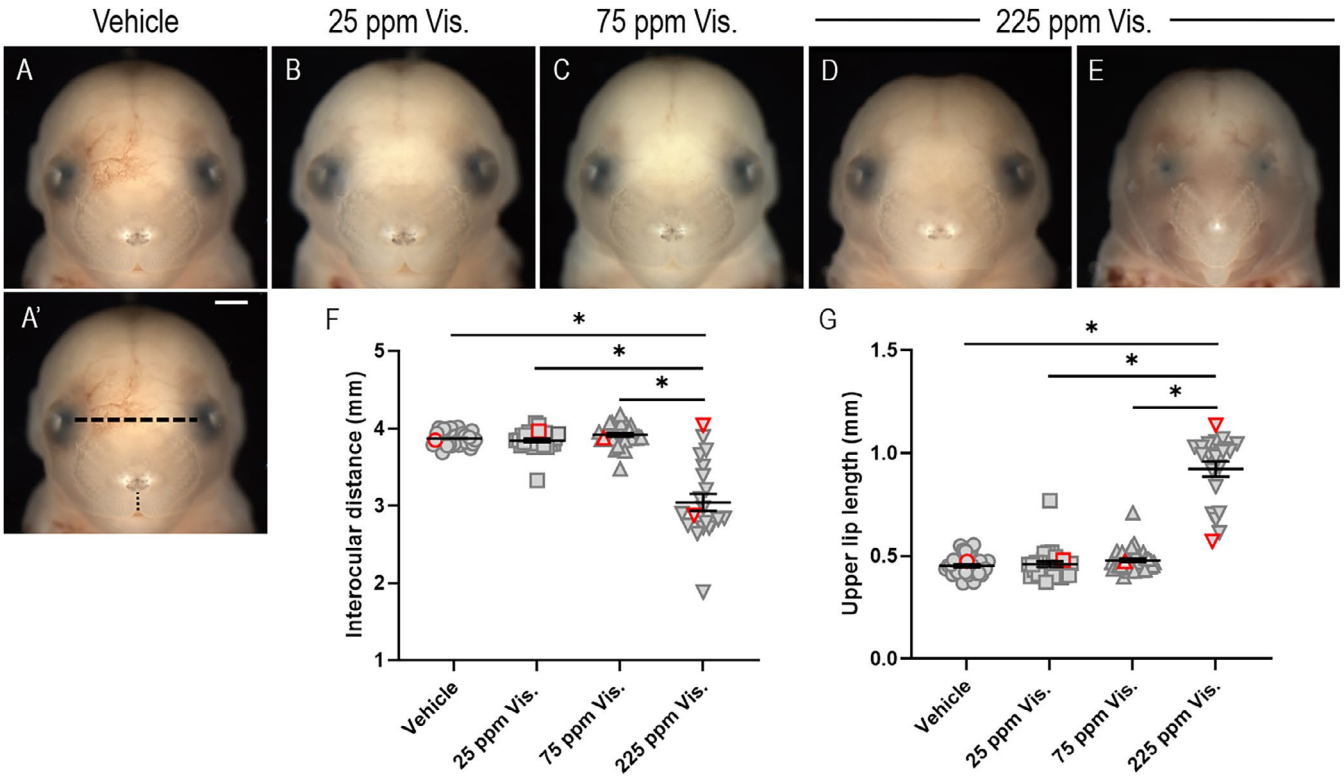

FIGURE 1 | Facial morphometric assessment in a dietary model of Shh pathway inhibition. (A–E) GD17 fetuses from dams fed vehicle- or vismodegib-containing chow at the indicated concentrations. Interocular distance (IOD) and upper lip length (ULL) measurements are represented visually in A′ by dashed and dotted lines, respectively. (F, G) Plots of IOD and ULL measurements in fetuses of dams fed vehicle chow ($n = 35$) or chow containing 25 ppm ($n = 28$), 75 ppm ($n = 36$), or 225 ppm ($n = 21$) vismodegib. Individual data points are plotted along with bars representing mean ± SEM. IOD and ULL measurements for the fetuses shown in panels A–E are indicated by red borders. One-way ANOVA with Tukey's post hoc test was used to compare the statistical significance of IOD and ULL measurements between treatment groups. *$p < 0.05$. Scale bar: 1 mm.

morphology that reflect the midline deficiency that defines this disorder (Everson et al. 2019; Heyne et al. 2016). Fetal mice were imaged at GD17, and IOD and ULL measurements were taken (Figure 1, additional annotated images in Figure S2). Litters exposed to 225 ppm vismodegib exhibited dysmorphic facial features consistent with HPE, such as decreased IOD and increased ULL, relative to all other treatment groups. Of note, while many fetuses within the 225 ppm treatment group exhibited severe phenotypes (i.e., overt midfacial hypoplasia and microcephaly in Figure 1E), a subset of samples exhibited mild forms of HPE (i.e., a shallow upper lip notch in Figure 1D). Mean values indicated no differences between vehicle-exposed fetuses and the 25 and 75 ppm treatment groups, though moderate HPE phenotypes were observed in single samples from these lower treatment groups (Figure S3). Additional Shh-associated limb defects were observed only in the 225 ppm treatment group (Figure S4). No craniofacial or limb defects were observed within the vehicle control group.

3.1.2 | Impacts on Brain Morphogenesis

Consistent with the results of the morphometric analysis, facial images showed no overt differences between vehicle-treated and 25 or 75 ppm vismodegib-treated fetuses, while the 225 ppm vismodegib diet induced HPE-like phenotypes with high penetrance (Figure 2A–E). Severe midfacial hypoplasia frequently co-occurred with microcephaly in the most affected animals (Figure 2E). One animal in the 225 ppm vismodegib group exhibited micrognathia without any obvious microcephaly (Figure 2D), again displaying a spectrum of phenotypic severity in the highest dose group. Disruption of Shh signaling during early neurodevelopment in mice causes various brain dysmorphologies, including hypoplasia or agenesis of the olfactory bulbs and incomplete forebrain division (Heyne et al. 2016; Heyne, Melberg, et al. 2015). In dissected brains, olfactory bulbs were comparable in size and position among vehicle and 25 and 75 ppm vismodegib treatment groups but diminished, unseparated, or even absent in the 225 ppm vismodegib group (Figure 2A′–E′). Incomplete cortical division was apparent in whole brains from severely affected animals in the 225 ppm vismodegib group. Coronal sections revealed that only treatment with 225 ppm vismodegib was sufficient to induce true HPE, with loss of forebrain division apparent in mice with overt midfacial hypoplasia (Figure 2A″–E″). Severity of forebrain and olfactory bulb abnormalities generally correlated with facial dysmorphology.

3.2 | Embryonic Forebrain Patterning Following Gestational Shh Pathway Antagonist Exposure

To test whether Shh pathway inhibition alters early forebrain patterning even at doses that do not produce overt craniofacial dysmorphology, embryos from dams provided control or 25, 75, or 225 ppm vismodegib diets were collected at GD11 for facial

imaging and ISH. Although resorptions were similar between treatment groups, litter size was reduced in the 25 ppm group but increased in the 75 ppm group. Embryos in the 75 and 225 ppm vismodegib groups were slightly smaller than the control embryos (Table 2).

Prior to staining, the rostral portion of each sample was imaged and hemisected along the sagittal plane to reveal early forebrain structures. ISH was used to visualize *Gli1*, a marker of Shh pathway activity, *Pax6*, a dorsal marker within the central nervous system, and *Nkx2-1*, a marker strongly expressed in the Shh-dependent MGE. Facial images showed no overt differences between the control group and the 25 and 75 ppm vismodegib groups, while embryos in the 225 ppm vismodegib group displayed phenotypes ranging from apparently normal to severely hypoplastic (Figure 3A–E). The same pattern was observed by ISH, with domains of localization for each marker remaining unchanged in the 25 ppm and 75 ppm vismodegib groups. Relative to the other groups, severely affected embryos from the 225 ppm vismodegib group exhibited reduced *Gli1* expression within the ventral forebrain and facial processes (Figure 3F–J), expanded *Pax6* expression into the ventral aspect of the forebrain (Figure 3K–O), and a greatly diminished or absent MGE based on *Nkx2-1* expression (Figure 3P–T). Measurements of the MGE, normalized to head size, revealed a significant decrease in the size of this structure in the 225 ppm vismodegib group (Figure 3U,V). As at later developmental stages, phenotypic variability was observed in facial images and ISH patterns among embryos in the 225 ppm vismodegib treatment group with a subset of samples exhibiting apparently normal facial features

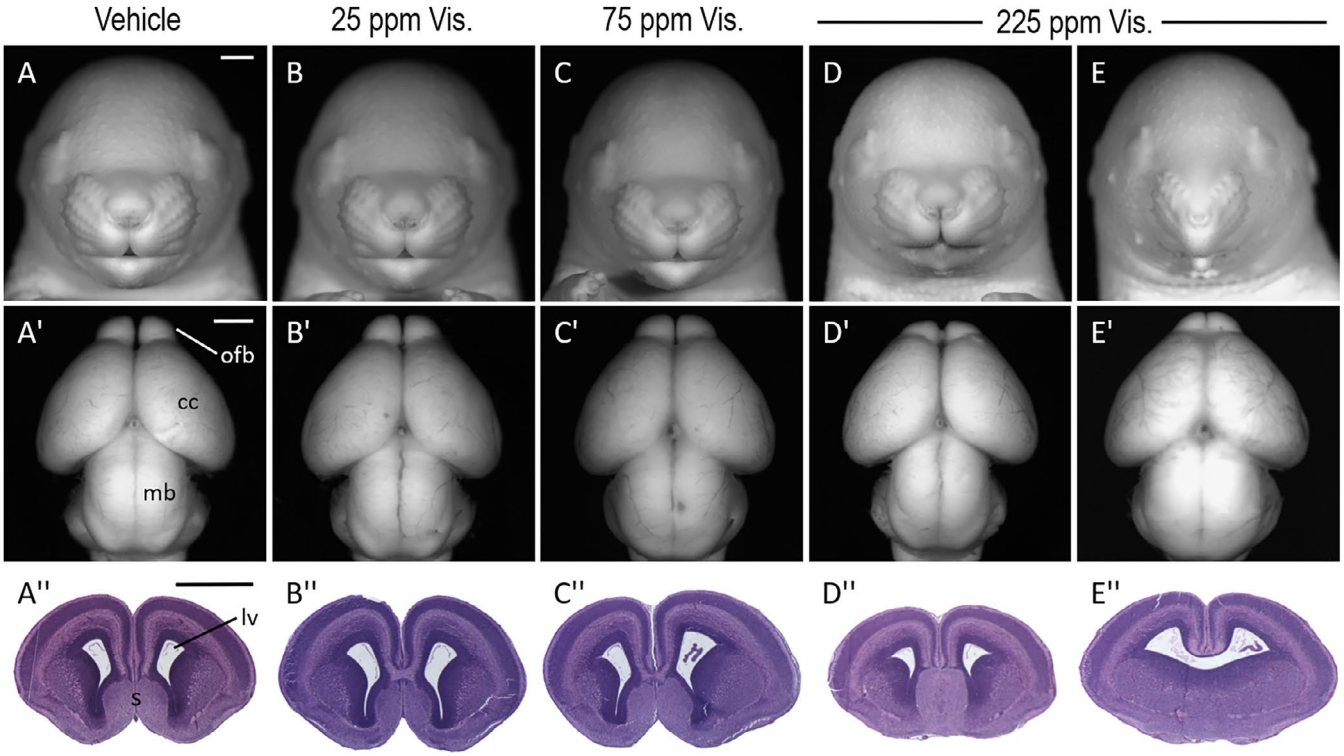

FIGURE 2 | Evaluation of face and brain morphology in fetal mice exposed to vismodegib. (A–E) Facial images of GD17 fetuses from dams fed diets containing vehicle ($n = 12$) or 25 ppm ($n = 20$), 75 ppm ($n = 19$), or 225 ppm ($n = 15$) vismodegib. Midfacial hypoplasia was apparent in most individuals from the highest exposure group. (A′–E′) Dorsal view of brains from the same individuals shown in A–E. Olfactory bulbs (ofb) were hypoplastic and partially unseparated following high vismodegib exposure, and the cerebral cortices (cc) showed only shallow divisions in the most severely affected samples. (A″–E″) H&E staining of coronal sections through the forebrain of the individuals in A–E. The 225 ppm vismodegib diet altered the size and shape of the lateral ventricles (lv) and septal region (s) in moderately affected samples (D″) and induced true HPE (incomplete separation of the forebrain) in severely affected samples (E″). mb, midbrain. Scale bars: 1 mm.

TABLE 2 | Litter statistics for GD11 embryos.

Treatment	Litters collected [*n*]	Viable embryos [*n* (mean)]	Resorptions [*n* (mean)]	Crown-rump [mean ± SD mm]
Vehicle	4	24 (6.0)	9 (2.3)	5.92 ± 0.24
25 ppm Vis.	3	12 (4.0)*	11 (3.7)	5.92 ± 0.29
75 ppm Vis.	3	26 (8.7)*	3 (1.0)	5.19 ± 0.65*
225 ppm Vis.	3	19 (6.3)	6 (2.0)	4.87 ± 1.05*

*$p < 0.05$.

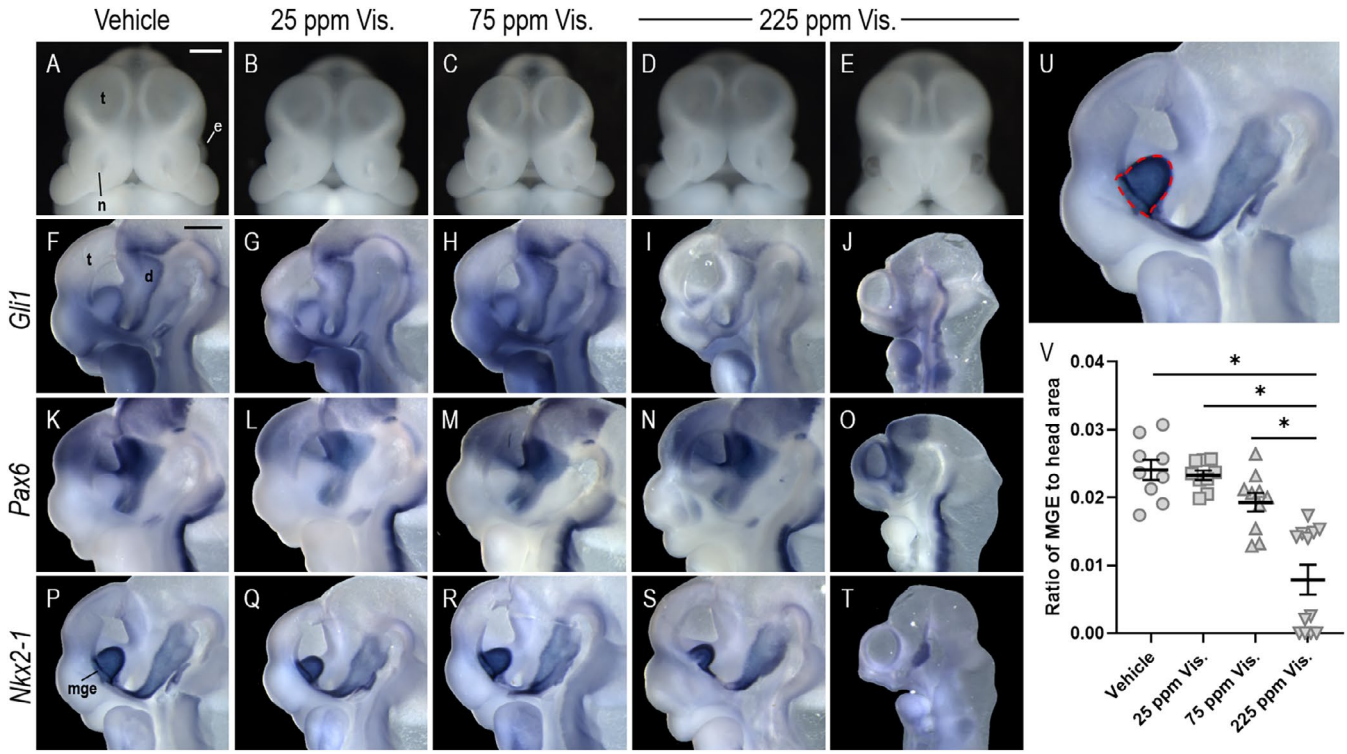

FIGURE 3 | Expression pattern of select genes within the forebrain of vismodegib-exposed embryos. (A–E) Representative frontal images of GD11 embryos from dams provided chow containing vehicle ($n = 24$) or 25 ppm ($n = 12$), 75 ppm ($n = 26$), or 225 ppm ($n = 19$) vismodegib. The 225 ppm vismodegib group showed varying degrees of midfacial hypoplasia resulting in closely approximated facial processes, eyes (e), nostrils (*n*), and telencephalic vesicles (t). (F–T) Embryos were bisected sagittally and stained using in situ hybridization for the genes indicated. In control samples, *Gli1* was most strongly expressed in the inferior aspect of the facial processes and dorsally into the diencephalon (d). *Pax6* was expressed dorsally within the telencephalon and diencephalon. *Nkx2-1* was expressed in the medial ganglionic eminence (mge) and the ventral diencephalon. (U) An enlarged view of panel Q with the measured area of the MGE outlined with a dashed red line. (V) Plot of MGE area normalized to head area for a subset of embryos from each litter; vehicle ($n = 9$), 25 ppm vismodegib ($n = 9$), 75 ppm vismodegib ($n = 10$), and 225 ppm vismodegib ($n = 12$). Individual samples are plotted, and bars represent the mean ± SEM. One-way ANOVA with Tukey's post hoc test was used to assess the statistical significance in MGE area. $^*p < 0.05$. Scale bars: 500 μm.

(Figure 3D) and intermediate differences in rostral *Gli1* and *Nkx2-1* patterning (Figure 3I,S). The domain of *Pax6* expression, however, was not clearly altered in the most normal individuals of the highest dose group (Figure 3N).

3.3 | Impact of Gestational Shh Pathway Antagonist Exposure on Behavior

We next examined the impact of prenatal vismodegib exposure on postnatal behavior using a battery of established assays. Viable litters could not be raised from the 225 ppm vismodegib group, so behavioral assays were conducted only in the vehicle and 25 and 75 ppm vismodegib groups. One to three male and female mice were taken from each litter, and six to seven litters were produced to attain the final sample size. The number of viable pups in each litter was consistent across treatment groups, as was the number of perinatal losses (Table 3). A treatment-dependent decrease in pup weight at the time of weaning was observed across all weaned mice. This trend remained when considering only mice that underwent testing, though the difference in the 25 ppm vismodegib treatment group was no longer significant. In total, 11 female and 12 male mice from the vehicle group underwent behavioral testing, and 12 females and 12 males underwent behavioral testing from both vismodegib-treated groups.

TABLE 3 | Population parameters for behavioral testing.

Treatment	Litters [*n*]	Viable pups [*n* (mean)]	Pups lost [*n* (mean)]	Mass at weaning [mean ± SD g]
Vehicle	6	34 (5.67)	4 (0.67)	10.86 ± 2.06
25 ppm Vis.	7	41 (5.86)	4 (0.57)	9.64 ± 1.51*
75 ppm Vis.	7	38 (5.43)	9 (1.29)	8.83 ± 2.06*

$^*p < 0.05$.

3.3.1 | Open Field

Following a week-long period of acclimation, adult mice were placed in an enclosed arena and allowed 30 min to move freely around the open field. A photobeam array was used to assess horizontal movement within the arena as well as vertical activity and stereotypic activity. Horizontal movement through the cage was

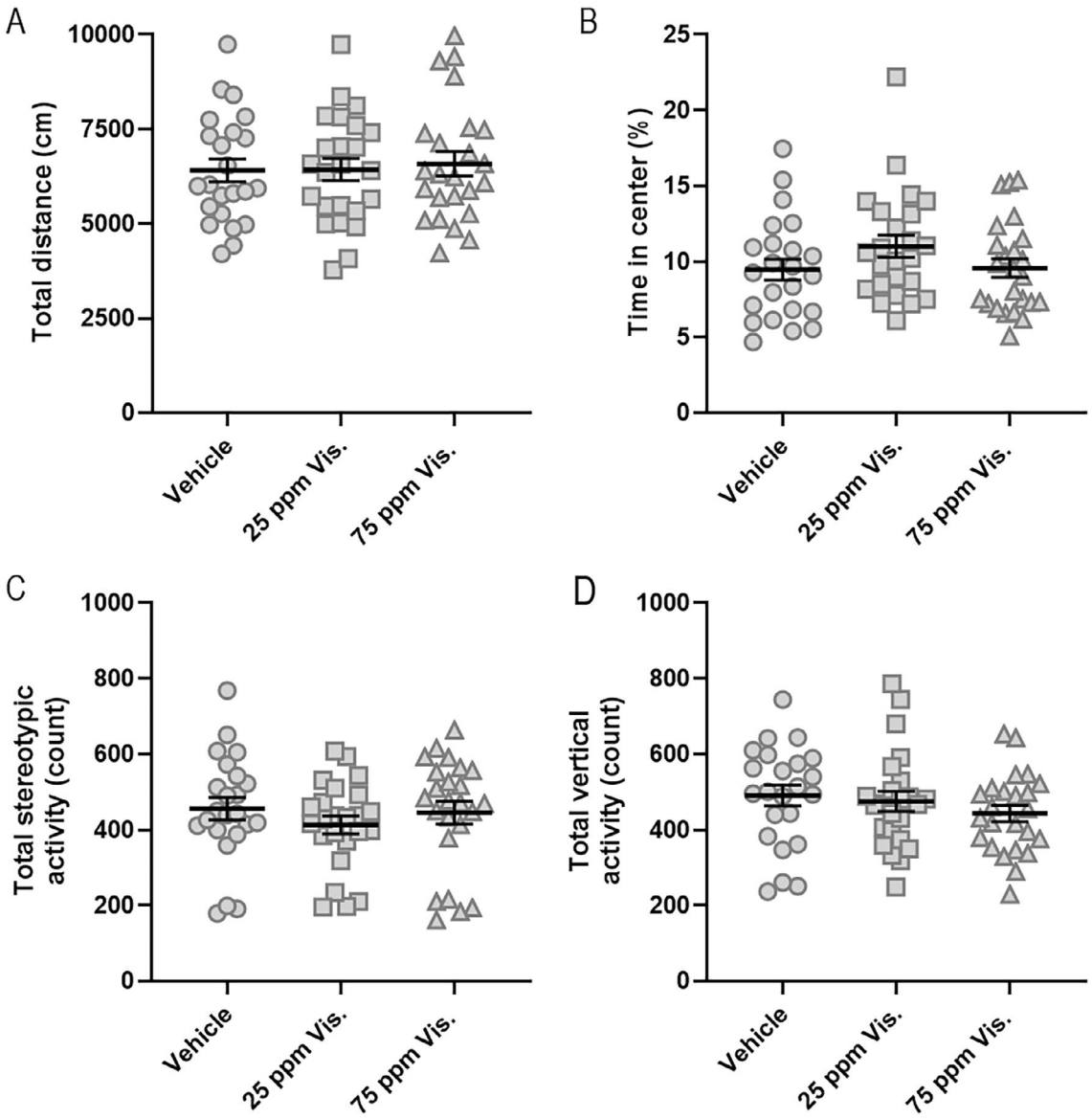

FIGURE 4 | Evaluation of open field exploration in adult mice with prenatal vismodegib exposure. (A–D) Plots of total distance traveled, the percentage of time spent in the center of the arena versus the peripheries, and counts of stereotypic behavior and vertical activity in mice from dams provided chow containing vehicle ($n = 23$) or 25 ppm ($n = 24$) or 75 ppm ($n = 24$) vismodegib. The 225 ppm vismodegib group was excluded from behavioral testing due to low litter viability. Data are presented as mean ± SEM. For statistical testing, time in center data were log-transformed to achieve a normal distribution. Stereotypic activity results failedShapiro-Wilk normality testing, so a nonparametric aligned rank transform was performed prior to analysis. Two-way ANOVA with Tukey's post hoc test was used to assess differences by treatment and sex.

used to assess total distance traveled and the proportion of time spent near the center of the cage versus the peripheries. Stereotypic activity was evaluated as repeated breaking of a single photobeam, and vertical movements were similarly tallied. No significant changes were observed in the total distance traveled, percent of time spent in the center of the arena, stereotypic behavior, or vertical activity when comparing treatment groups (Figure 4). A sex-dependent difference was seen only in vertical activity, with males engaging in more vertical activity than females (Figure S5).

3.3.2 | Marble Burying

In the marble burying assay, individual mice were placed in an arena with 20 marbles arrayed over a thick layer of bedding. After 30 min, mice were removed from the arena, and the number of fully buried marbles was counted. There were no treatment-dependent differences in the number of marbles buried (Figure 5), though there was a significant difference in marble burying between males and females (Figure S6).

3.3.3 | Rotarod

Four sessions of rotarod testing were performed to investigate motor coordination and memory acquisition across treatment groups. Mice were placed on a rotating rod that increased from 4 rpm to 40 rpm over the 5-min test. Significant effects of treatment, sex, and session, as well as their interactions, were observed. Session 4 was found to significantly differ from

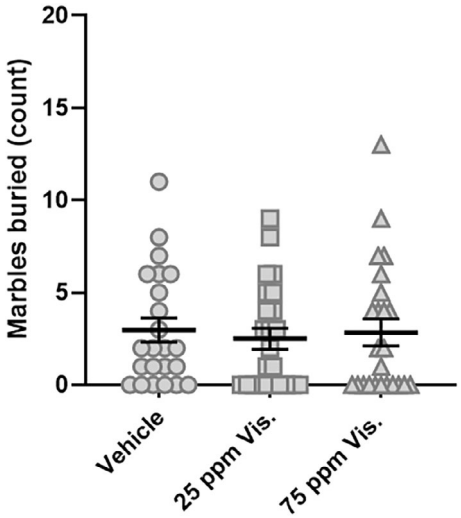

FIGURE 5 | Marble burying behavior in adult mice with prenatal vismodegib exposure. The number of marbles buried by mice prenatally exposed to diets containing vehicle ($n = 23$) or 25 ppm ($n = 24$) or 75 ppm ($n = 24$) vismodegib. Data are presented as mean ± SEM. The data failed Shapiro–Wilk normality testing, so a nonparametric aligned rank transform two-way ANOVA with post hoc test was used to assess differences by treatment and sex.

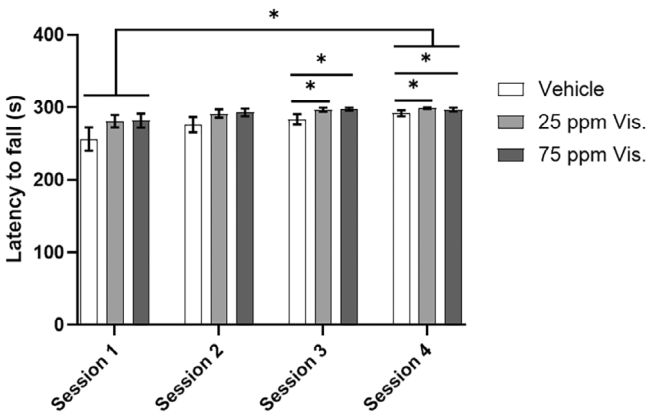

FIGURE 6 | Rotarod performance in adult mice with prenatal vismodegib exposure. Mice prenatally exposed to diets containing vehicle ($n = 23$) or 25 ppm ($n = 24$) or 75 ppm ($n = 24$) vismodegib were placed on a rotarod apparatus for four sessions, and the time it took for mice to fall from the apparatus was recorded. Many mice from each treatment group successfully remained on the rotarod for the full duration of each 300-s session. Values represent the mean ± SEM for each treatment and session. The data failed Shapiro–Wilk normality testing, so a nonparametric aligned rank transform ANOVA with post hoc test was used to compare differences between treatment groups, sexes, and sessions. Treatment-dependent changes are indicated within sessions, and a session-dependent difference was observed between the first and fourth sessions. *$p < 0.05$.

session 1, indicating that assay performance improved with repetition (Figure 6). Treatment-related effects were observed only in the third and fourth sessions, with vismodegib-treated mice outperforming the vehicle-exposed mice (Figure 6). Of note, C57BL/6J mice have a high baseline performance in the rotarod assay, consistent with the results of the first session in which mice across all treatment groups remained on the rotarod for an average of 273.3 s of the 300-s assay. The improvement in rotarod performance observed in the vismodegib-exposed animals did not align with expectations. However, given the limited variability observed within this assay (i.e., the majority of mice tested remained on the rotarod for the entire duration of each session) and the modest nominal increase in latency to fall, this finding should be interpreted with caution. Across all treatment groups and sessions, males remained on the rotarod for 289.7 ± 2.7 s compared to 284.9 ± 3.6 s for females (Supplemental Figure 7).

3.3.4 | Olfactory Discrimination and Detection

Olfactory discrimination was probed over two phases by comparing time spent investigating a novel scent versus a familiar scent. In the first session, mice were placed in a cage containing swabs dampened with water (familiar scent) or either mint or lemon extract (novel scent). During the second session, the swabs were dampened with each of the extracts, one familiarized during the first session and the other novel. Time spent investigating each swab was again recorded. Surprisingly, though there were no sex- or treatment-dependent effects, mice showed a preference for water (4.0 ± 0.6 s) over the novel scents (2.1 ± 0.2 s) in the first phase of testing (Figure 7A). No treatment-dependent differences in preference for the novel or familiar scents were observed in the second phase, nor were there sex-dependent effects (Figure S8A). To test whether these unexpected responses to novel scents indicated a general dysfunction in olfaction, the mice were also evaluated for their ability to detect an object buried under cage bedding. The ability of treated mice to detect odors was evaluated as the latency to find the scented object. No differences were observed between treatment groups in the olfactory detection assay, though all but one mouse was able to find the buried object during the 300 s testing window (Figure 7B). Additionally, there were no differences between sexes in olfactory detection (Figure S8B).

3.3.5 | Fear Conditioning

Finally, the fear conditioning assay was employed as a well-established test of memory and learning. Following a training session in which mice experienced two CS-US pairings that induced freezing, contextual fear recall and cued fear recall tests were administered. No treatment-dependent differences in time spent freezing were observed when mice were placed into the fear conditioning chamber to assess contextual fear recall (Figure 8A). In the cued fear recall test, the fear conditioning chamber was modified to create a novel visual and olfactory context for the subjects. During cued fear recall testing sessions, the CS alone was administered twice and freezing during each 30-s event was recorded. All groups exhibited elevated freezing during the second CS event relative to the first. During the first CS event, the 25 ppm vismodegib treatment group froze for significantly longer than the 75 ppm vismodegib treatment group, though neither treatment resulted in significant differences relative to the vehicle control mice (Figure 8B). No treatment-dependent differences were observed during the

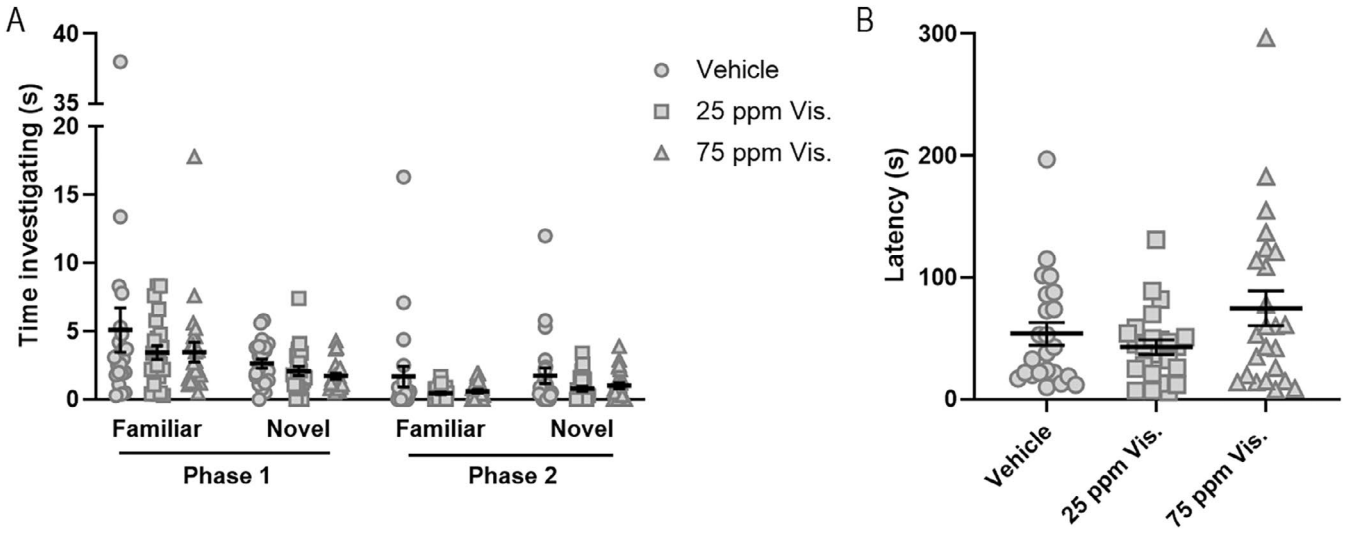

FIGURE 7 | Assessment of olfactory detection and discrimination in adult mice exposed prenatally to vismodegib. (A) Olfactory discrimination in mice prenatally exposed to diets containing vehicle ($n = 23$) or 25 ppm ($n = 24$) or 75 ppm ($n = 24$) vismodegib was evaluated in two phases. In the first phase, the amount of time mice spent investigating a swab scented with water (familiar) or a swab scented with either lemon or mint (novel) was recorded. During the second phase, mice were provided with two scented swabs, one with the now familiar scent from phase one and the other with a novel scent. The amount of time spent investigating each swab was again recorded. (B) The latency to find a scented object buried beneath bedding was used to evaluate the ability of treated mice to detect odors. Data are presented as mean ± SEM. For olfactory discrimination, the data failed Shapiro–Wilk normality testing, so a nonparametric aligned rank transform ANOVA with post hoc test was used to compare differences by treatment group, sexes, and scent within each session. Olfactory detection data were log-normalized to achieve a normal distribution, and two-way ANOVA with Tukey's post hoc test was used to assess differences by treatment and sex.

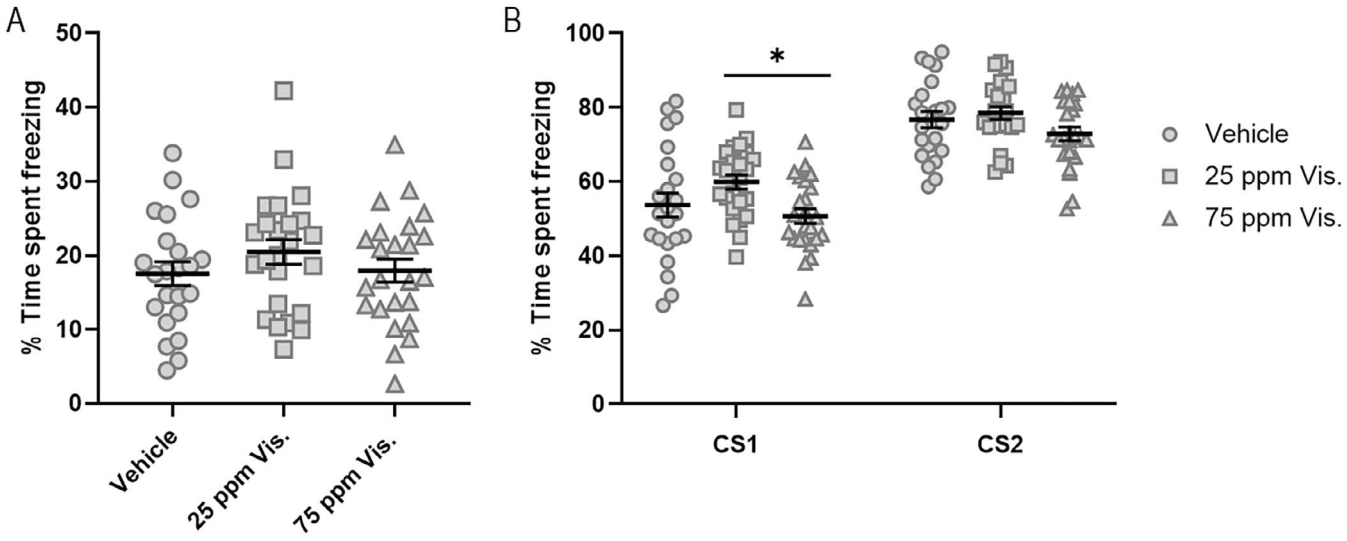

FIGURE 8 | Fear conditioning behavior in adult mice exposed prenatally to vismodegib. (A) To test contextual fear recall, mice prenatally exposed to diets of vehicle ($n = 23$) or 25 ppm ($n = 24$) or 75 ppm ($n = 24$) vismodegib were placed in the same fear conditioning chamber in which they first experienced the CS-US pairing 22 h prior, and time spent freezing was recorded over a 360-s period. (B) Cued fear recall was assessed by administering the CS only to mice in a novel context 24 h after the CS-US training. Time spent freezing during each 30 s CS event was recorded. Bars represent mean ± SEM. Two-way ANOVA with Tukey's post hoc test was used to assess differences by treatment and sex. *$p < 0.05$.

second CS event, and there was no effect of sex on fear conditioning (Figure S9).

4 | Discussion

Defining the molecular pathways that drive NDD pathogenesis is critical for preventing these etiologically complex diseases. To our knowledge, the study reported herein is the first to investigate neurobehavioral effects following low-dose Shh signaling disruption spanning the critical period for craniofacial morphogenesis. The pharmacological hedgehog pathway inhibitor vismodegib was selected for this study due to its specificity, potency, and short half-life, allowing for selective inhibition of the Shh pathway between GD4 and GD12 with minimal off-target toxic effects (Robarge et al. 2009; Wong et al. 2011, 2009).

Gestational exposure to the 225 ppm vismodegib diet produced a spectrum of face and forebrain phenotypes of varying severity and was incompatible with postnatal survival. Surprisingly, consumption of chow containing 25 or 75 ppm vismodegib had no apparent impact on early forebrain patterning at GD11 or gross morphology of the face or forebrain at GD17. Adult mice that were prenatally exposed to 25 or 75 ppm vismodegib were phenotypically normal and did not exhibit robust behavioral differences in the battery of assays conducted in this study.

The potential for small molecule Shh pathway inhibitors to disrupt neurodevelopment without producing overt external dysmorphologies has critical implications for our understanding of NDD pathogenesis, broadening the spectrum of adverse outcomes that may otherwise go unnoticed due to a focus primarily on external anomalies. The expansion of fetal alcohol spectrum disorders (FASD) to include individuals with neurobehavioral symptoms who lack external dysmorphologies provides a salient comparison. Studies in recent decades reveal a more substantial role of prenatal alcohol exposure in neurodevelopment than was previously recognized by identifying adverse neurobehavioral outcomes in children who appear phenotypically normal (Coles et al. 2020; Hoyme et al. 2016, 2005).

A role for low-dose Shh signaling inhibition in the disruption of early neurodevelopment was previously posited. One notable study investigated the capacity for piperonyl butoxide (PBO), a pesticide synergist and Shh pathway inhibitor (Rivera-González et al. 2021; Wang et al. 2012), to cause Shh-associated malformations in mice. The authors found that the MGE and septal region of the forebrain were diminished following doses of PBO that caused only subtle facial dysmorphology (Everson et al. 2019). Extrapolating to a human population in which normal face shape variation may mask subtle abnormalities, these results suggest that low levels of Shh signaling disruption may impact neurodevelopment without overtly altering facial morphogenesis (Hammond and Suttie 2012; Hoyme et al. 2015). Under the experimental conditions examined in this study, brain anomalies were not observed in the absence of robust craniofacial anomalies. Several factors, such as the use of a dietary model of inhibition rather than an acute oral dose or differences in the specificity and potency of vismodegib and PBO as Shh pathway antagonists, may explain the seemingly disparate results between these studies.

Research from a separate lab demonstrated neurobehavioral changes in mice following gestational and lactational exposure to PBO through modified diets (Tanaka 2003; Tanaka and Inomata 2015, 2016; Tanaka et al. 2009). Significant changes in offspring mice were observed in measures of motor coordination, exploratory behavior, spontaneous behavior, and olfaction, though treatment paradigms and neurobehavioral results were not consistent across all studies. Furthermore, the studies were not designed to interrogate underlying mechanisms. The exposure models presented by Tanaka and colleagues most closely match the dietary vismodegib model utilized herein (Tanaka 2003; Tanaka and Inomata 2015, 2016; Tanaka et al. 2009). However, that PBO exposure in each study spanned, at minimum, gestation and lactation may explain the subtler phenotypes observed by Tanaka et al. Furthermore, PBO's impacts are not limited solely to Shh pathway inhibition, and additional studies using specific antagonists, such as vismodegib, over a broader period of development will clarify whether Shh signaling disruption alone can induce neurobehavioral deficits in the absence of overt dysmorphology.

We designed this study to expose mice over a period spanning the critical period for HPE, providing vismodegib-laced diets from GD4 to GD12 (Heyne, Melberg, et al. 2015), roughly corresponding to the first 6 weeks in human gestation. This developmental period is highly dynamic and encompasses several, but not all, key roles of Shh signaling in brain morphogenesis and CNS development. For example, Shh is implicated in oligodendrogenesis in both the ventral and dorsal forebrain after GD12 in mice (Machold et al. 2003; Winkler et al. 2018; Zhang et al. 2020). In addition, oligodendrocyte and astrocyte differentiation were modulated based on Shh pathway activity in primary rodent neural cell culture models of gliogenesis (Araújo et al. 2014; Wang and Almazan 2016). Whether targeted disruption of Shh during later stages in neurodevelopment can induce behavioral changes through altered gliogenesis or other mechanisms in the absence of overt malformations remains unknown. Similarly, future studies investigating low-dose Shh signaling disruption may extend the window of treatment to encompass the murine equivalents of neurodevelopment during the second and third trimesters in humans, which extends into the early postnatal period in mice (Almeida et al. 2020; Parnell et al. 2014).

This study was constrained by several limitations. To reduce variability in the experimental design, litters were generated for each treatment group and endpoint concurrently. Therefore, additional treatment groups could not be added without potentially introducing a group-specific bias. The absence of a treatment group that consistently induced HPE with low penetrance prevented the assessment of neurobehavioral changes in apparently normal littermates of overtly affected individuals. Whether the treatment paradigm employed herein can induce mild or low-penetrance facial dysmorphology requires additional study. Furthermore, practical considerations limited the number of neurobehavioral tests that were conducted. The behavioral assays utilized, though not comprehensive in scope, were selected for their breadth due to limited reports of neurobehavioral impacts of gestational Shh pathway disruption. The finding of diminished MGE size in the 225 ppm vismodegib group can inform future studies on behavioral impacts of Shh disruption. The MGE, a transient forebrain structure, gives rise to cortical interneurons. This subset of neurons is implicated in diseases such as epilepsy, schizophrenia, and autism, as well as deficits in social behavior (reviewed in (Ansen-Wilson and Lipinski 2017; Katsarou et al. 2017)). In addition to effects on the MGE, research has also found altered Shh levels in neurological conditions including autism spectrum disorder, Parkinson's Disease, epilepsy, and demyelinating diseases such as multiple sclerosis (Al-Ayadhi 2012; Dhekne et al. 2018; Fang et al. 2011; Feng et al. 2016; Mastronardi et al. 2003). A role for Shh in the pathogenesis of these disorders has not been fully elucidated, but future efforts may leverage behavioral and functional assays targeting specific disease outcomes to support a causative or predisposing effect of prenatal Shh disruption in NDD pathogenesis.

The dietary model of Shh pathway inhibition presented herein also possesses strengths. In both the human population and

animal models, HPE presents with incomplete penetrance and phenotypic variability (Tekendo-Ngongang et al. 2020). Although HPE is most often embryonic lethal (Matsunaga and Shiota 1977; Orioli and Castilla 2010), individuals living with HPE-associated variants span the spectrum from phenotypically normal to mild midfacial hypoplasia (i.e., a single central top incisor) to more moderate and severe midfacial and forebrain hypoplasia (i.e., hypotelorism, microcephaly). HPE-related neurobehavioral impacts cover a similarly broad spectrum from normal brain function to cognitive delay to substantial impairment. Generally, the severity of facial and brain defects is closely correlated, inspiring the aphorism "the face predicts the brain" (DeMyer et al. 1964). The dietary Shh disruption model presented in this study recapitulates this phenotypic variability as well as the established correlation between face and forebrain outcomes. Leveraging this phenotypic variability and the low-stress exposure paradigm, the dietary vismodegib model is suitable for study of multifactorial insult including gene–environment and environment–environment interactions. Combining simultaneous environmental insult or predisposing genetic variations with the vismodegib diet can inform the impact of Shh modulation on multifactorial NDDs. This model has the potential to be a powerful tool for exploring etiologically complex developmental disorders.

This study was designed to address whether Shh signaling pathway disruption alters neurodevelopment in the absence of overt facial dysmorphology. Resolving this question is critical to the informed assessment of health hazards in the context of environmental Shh pathway inhibition. The current study did not support a model of NDD pathogenesis in which Shh pathway disruption can significantly impact neurodevelopment without altering craniofacial or limb morphogenesis, though future research may further clarify the impact of low-dose Shh disruption on NDD outcomes by examining more intermediate doses of vismodegib, a broader spectrum of behavioral endpoints, or expanding the period of Shh pathway disruption to target additional critical periods of development.

Acknowledgments

The authors acknowledge the Biomedical Research Model Services at the University of Wisconsin-Madison for careful management of our mouse colonies. The authors also thank Dr. Michael Cahill for thoughtful discussion of the behavioral approaches employed in this study.

Conflicts of Interest

The authors declare no conflicts of interest.

Data Availability Statement

The data that support the findings of this study are available from the corresponding author upon reasonable request.

References

Abler, L. L., V. Mehta, K. P. Keil, et al. 2011. "A High Throughput In Situ Hybridization Method to Characterize mRNA Expression Patterns in the Fetal Mouse Lower Urogenital Tract." *Journal of Visualized Experiments* no. 54: e2912. https://doi.org/10.3791/2912.

Addissie, Y. A., A. Troia, Z. C. Wong, et al. 2021. "Identifying Environmental Risk Factors and Gene–Environment Interactions in Holoprosencephaly." *Birth Defects Research* 113, no. 1: 63–76. https://doi.org/10.1002/bdr2.1834.

Al-Ayadhi, L. Y. 2012. "Relationship Between Sonic Hedgehog Protein, Brain-Derived Neurotrophic Factor and Oxidative Stress in Autism Spectrum Disorders." *Neurochemical Research* 37, no. 2: 394–400. https://doi.org/10.1007/s11064-011-0624-x.

Almeida, L., V. Andreu-Fernández, E. Navarro-Tapia, et al. 2020. "Murine Models for the Study of Fetal Alcohol Spectrum Disorders: An Overview." *Frontiers in Pediatrics* 8: 359. https://doi.org/10.3389/fped.2020.00359.

Ansen-Wilson, L. J., and R. J. Lipinski. 2017. "Gene-Environment Interactions in Cortical Interneuron Development and Dysfunction: A Review of Preclinical Studies." *Neurotoxicology* 58: 120–129.

Araújo, G. L., J. A. Araújo, T. Schroeder, A. B. Tort, and M. R. Costa. 2014. "Sonic Hedgehog Signaling Regulates Mode of Cell Division of Early Cerebral Cortex Progenitors and Increases Astrogliogenesis." *Frontiers in Cellular Neuroscience* 8: 1–11.

Britto, J., D. Tannahill, and R. Keynes. 2002. "A Critical Role for Sonic Hedgehog Signaling in the Early Expansion of the Developing Brain." *Nature Neuroscience* 5, no. 2: 103–110. https://doi.org/10.1038/nn797.

Butt, S. J. B., M. Fuccillo, S. Nery, et al. 2005. "The Temporal and Spatial Origins of Cortical Interneurons Predict Their Physiological Subtype." *Neuron* 48, no. 4: 591–604. https://doi.org/10.1016/j.neuron.2005.09.034.

Chen, J. K. 2016. "I Only Have Eye for Ewe: The Discovery of Cyclopamine and Development of Hedgehog Pathway-Targeting Drugs." *Natural Product Reports* 33, no. 5: 595–601. https://doi.org/10.1039/c5np00153f.

Chiang, C., Y. Litingtung, E. Lee, et al. 1996. "Cyclopia and Defective Axial Patterning in Mice Lacking Sonic Hedgehog Gene Function." *Nature* 383, no. 6599: 407–413. https://doi.org/10.1038/383407a0.

Coles, C. D., W. Kalberg, J. A. Kable, B. Tabachnick, P. A. May, and C. D. Chambers. 2020. "Characterizing Alcohol-Related Neurodevelopmental Disorder: Prenatal Alcohol Exposure and the Spectrum of Outcomes." *Alcoholism: Clinical and Experimental Research* 44, no. 6: 1245–1260. https://doi.org/10.1111/acer.14325.

De Felice, A., L. Ricceri, A. Venerosi, F. Chiarotti, and G. Calamandrei. 2015. "Multifactorial Origin of Neurodevelopmental Disorders: Approaches to Understanding Complex Etiologies." *Toxics* 3, no. 1: 89–129.

DeMyer, W., W. Zeman, and C. G. Palmer. 1964. "The Face Predicts the Brain: Diagnostic Significance of Median Facial Anomalies for Holoprosencephaly (Arhinencephaly)." *Pediatrics* 34: 256–263.

Dhekne, H. S., I. Yanatori, R. C. Gomez, et al. 2018. "A Pathway for Parkinson's Disease LRRK2 Kinase to Block Primary Cilia and Sonic Hedgehog Signaling in the Brain." *eLife* 7: e40202. https://doi.org/10.7554/eLife.40202.

Dubourg, C., A. Kim, E. Watrin, et al. 2018. "Recent Advances in Understanding Inheritance of Holoprosencephaly." *American Journal of Medical Genetics Part C Seminar in Medical Genetics* 178, no. 2: 258–269. https://doi.org/10.1002/ajmg.c.31619.

Elkin, L. A., M. Kay, J. J. Higgins, and J. O. Wobbrock. 2021. "An Aligned Rank Transform Procedure for Multifactor Contrast Tests." *The 34th Annual ACM Symposium on User Interface Software and Technology, Virtual Event, USA*. https://doi.org/10.1145/3472749.3474784.

Ericson, J., J. Muhr, M. Placzek, T. Lints, T. M. Jessel, and T. Edlund. 1995. "Sonic Hedgehog Induces the Differentiation of Ventral Forebrain Neurons: A Common Signal for Ventral Patterning Within the Neural Tube." *Cell* 81, no. 5: 747–756. https://doi.org/10.1016/0092-8674(95)90536-7.

Everson, J. L., M. R. Sun, D. M. Fink, et al. 2019. "Developmental Toxicity Assessment of Piperonyl Butoxide Exposure Targeting Sonic Hedgehog

Signaling and Forebrain and Face Morphogenesis in the Mouse: An In Vitro and In Vivo Study." *Environmental Health Perspectives* 127, no. 10: 107006. https://doi.org/10.1289/EHP5260.

Fang, M., Y. Lu, G. J. Chen, L. Shen, Y. M. Pan, and X. F. Wang. 2011. "Increased Expression of Sonic Hedgehog in Temporal Lobe Epileptic Foci in Humans and Experimental Rats." *Neuroscience* 182: 62–70. https://doi.org/10.1016/j.neuroscience.2011.02.060.

Feng, S., S. Ma, C. Jia, et al. 2016. "Sonic Hedgehog Is a Regulator of Extracellular Glutamate Levels and Epilepsy." *EMBO Reports* 17, no. 5: 682–694. https://doi.org/10.15252/embr.201541569.

Fuccillo, M., M. Rallu, A. P. McMahon, and G. Fishell. 2004. "Temporal Requirement for Hedgehog Signaling in Ventral Telencephalic Patterning." *Development* 131, no. 20: 5031–5040. https://doi.org/10.1242/dev.01349.

Furuta, Y., D. W. Piston, and B. L. M. Hogan. 1997. "Bone Morphogenetic Proteins (BMPs) as Regulators of Dorsal Forebrain Development." *Development* 124, no. 11: 2203–2212. https://doi.org/10.1242/dev.124.11.2203.

Hammond, P., and M. Suttie. 2012. "Large-Scale Objective Phenotyping of 3D Facial Morphology." *Human Mutation* 33: 817–825. https://doi.org/10.1002/humu.22054.

Heyne, G. W., J. L. Everson, L. J. Ansen-Wilson, et al. 2016. "Gli2 Gene-Environment Interactions Contribute to the Etiological Complexity of Holoprosencephaly: Evidence From a Mouse Model." *Disease Models & Mechanisms* 9, no. 11: 1307–1315. https://doi.org/10.1242/dmm.026328.

Heyne, G. W., C. G. Melberg, P. Doroodchi, et al. 2015. "Definition of Critical Periods for Hedgehog Pathway Antagonist-Induced Holoprosencephaly, Cleft Lip, and Cleft Palate." *PLoS One* 10, no. 3: e0120517. https://doi.org/10.1371/journal.pone.0120517.

Heyne, G. W., E. H. Plisch, C. G. Melberg, E. P. Sandgren, J. A. Peter, and R. J. Lipinski. 2015. "A Simple and Reliable Method for Early Pregnancy Detection in Inbred Mice." *Journal of the American Association for Laboratory Animal Science* 54, no. 4: 368–371.

Hong, M., and R. S. Krauss. 2012. "Cdon Mutation and Fetal Ethanol Exposure Synergize to Produce Midline Signaling Defects and Holoprosencephaly Spectrum Disorders in Mice." *PLoS Genetics* 8, no. 10: e1002999. https://doi.org/10.1371/journal.pgen.1002999.

Hong, M., and R. S. Krauss. 2018. "Modeling the Complex Etiology of Holoprosencephaly in Mice." *American Journal of Medical Genetics. Part C, Seminars in Medical Genetics* 178, no. 2: 140–150. https://doi.org/10.1002/ajmg.c.31611.

Hoyme, H. E., D. B. Hoyme, A. J. Elliott, et al. 2015. "A South African Mixed Race Lip/Philtrum Guide for Diagnosis of Fetal Alcohol Spectrum Disorders." *American Journal of Medical Genetics Part A* 167, no. 4: 752–755. https://doi.org/10.1002/ajmg.a.37023.

Hoyme, H. E., W. O. Kalberg, A. J. Elliott, et al. 2016. "Updated Clinical Guidelines for Diagnosing Fetal Alcohol Spectrum Disorders." *Pediatrics* 138, no. 2: e20154256. https://doi.org/10.1542/peds.2015-4256.

Hoyme, H. E., P. A. May, W. O. Kalberg, et al. 2005. "A Practical Clinical Approach to Diagnosis of Fetal Alcohol Spectrum Disorders: Clarification of the 1996 Institute of Medicine Criteria." *Pediatrics* 115, no. 1: 39–47. https://doi.org/10.1542/peds.2004-0259.

Jeong, J., J. Mao, T. Tenzen, A. H. Kottmann, and A. P. McMahon. 2004. "Hedgehog Signaling in the Neural Crest Cells Regulates the Patterning and Growth of Facial Primordia." *Genes & Development* 18, no. 8: 937–951. https://doi.org/10.1101/gad.1190304.

Katsarou, A. M., S. L. Moshé, and A. S. Galanopoulou. 2017. "Interneuronopathies and Their Role in Early Life Epilepsies and Neurodevelopmental Disorders." *Epilepsia Open* 2, no. 3: 284–306. https://doi.org/10.1002/epi4.12062.

Lan, A., M. Kalimian, B. Amram, and O. Kofman. 2017. "Prenatal Chlorpyrifos Leads to Autism-Like Deficits in C57Bl6/J Mice." *Environmental Health* 16, no. 1: 43. https://doi.org/10.1186/s12940-017-0251-3.

Lyall, K., L. Croen, J. Daniels, et al. 2017. "The Changing Epidemiology of Autism Spectrum Disorders." *Annual Review of Public Health* 38: 81–102. https://doi.org/10.1146/annurev-publhealth-031816-044318.

Machold, R., S. Hayashi, M. Rutlin, et al. 2003. "Sonic Hedgehog Is Required for Progenitor Cell Maintenance in Telencephalic Stem Cell Niches." *Neuron* 39, no. 6: 937–950. https://doi.org/10.1016/S0896-6273(03)00561-0.

Mastronardi, F. G., L. A. G. daCruz, H. Wang, J. Boggs, and M. A. Moscarello. 2003. "The Amount of Sonic Hedgehog in Multiple Sclerosis White Matter Is Decreased and Cleavage to the Signaling Peptide Is Deficient." *Multiple Sclerosis Journal* 9, no. 4: 362–371. https://doi.org/10.1191/1352458503ms924oa.

Matsunaga, E., and K. Shiota. 1977. "Holoprosencephaly in Human Embryos: Epidemiologic Studies of 150 Cases." *Teratology* 16, no. 3: 261–272. https://doi.org/10.1002/tera.1420160304.

Orioli, I. M., and E. E. Castilla. 2010. "Epidemiology of Holoprosencephaly: Prevalence and Risk Factors." *American Journal of Medical Genetics. Part C, Seminars in Medical Genetics* 154C, no. 1: 13–21. https://doi.org/10.1002/ajmg.c.30233.

Parnell, S. E., H. E. Holloway, L. K. Baker, M. A. Styner, and K. K. Sulik. 2014. "Dysmorphogenic Effects of First Trimester-Equivalent Ethanol Exposure in Mice: A Magnetic Resonance Microscopy-Based Study." *Alcoholism, Clinical and Experimental Research* 38, no. 7: 2008–2014. https://doi.org/10.1111/acer.12464.

Petryk, A., D. Graf, and R. Marcucio. 2015. "Holoprosencephaly: Signaling Interactions Between the Brain and the Face, the Environment and the Genes, and the Phenotypic Variability in Animal Models and Humans." *Wiley Interdisciplinary Reviews: Developmental Biology* 4, no. 1: 17–32. https://doi.org/10.1002/wdev.161.

Richieri-Costa, A., and L. A. Ribeiro. 2010. "Holoprosencephaly and Holoprosencephaly-Like Phenotypes: Review of Facial and Molecular Findings in Patients From a Craniofacial Hospital in Brazil." *American Journal of Medical Genetics. Part C, Seminars in Medical Genetics* 154C, no. 1: 149–157. https://doi.org/10.1002/ajmg.c.30247.

Rivera-González, K. S., T. G. Beames, and R. J. Lipinski. 2021. "Examining the Developmental Toxicity of Piperonyl Butoxide as a Sonic Hedgehog Pathway Inhibitor." *Chemosphere* 264, no. Pt 1: 128414. https://doi.org/10.1016/j.chemosphere.2020.128414.

Robarge, K. D., S. A. Brunton, G. M. Castanedo, et al. 2009. "GDC-0449-A Potent Inhibitor of the Hedgehog Pathway." *Bioorganic & Medicinal Chemistry Letters* 19, no. 19: 5576–5581. https://doi.org/10.1016/j.bmcl.2009.08.049.

Roelink, H., J. A. Porter, C. Chiang, et al. 1995. "Floor Plate and Motor Neuron Induction by Different Concentrations of the Amino-Terminal Cleavage Product of Sonic Hedgehog Autoproteolysis." *Cell* 81, no. 3: 445–455. https://doi.org/10.1016/0092-8674(95)90397-6.

Roessler, E., E. Belloni, K. Gaudenz, et al. 1996. "Mutations in the Human Sonic Hedgehog Gene Cause Holoprosencephaly." *Nature Genetics* 14, no. 3: 357–360. https://doi.org/10.1038/ng1196-357.

Solomon, B. D., K. A. Bear, A. Wyllie, et al. 2012. "Genotypic and Phenotypic Analysis of 396 Individuals With Mutations in Sonic Hedgehog." *Journal of Medical Genetics* 49, no. 7: 473–479. https://doi.org/10.1136/jmedgenet-2012-101008.

Tanaka, T. 2003. "Reproductive and Neurobehavioural Effects of Piperonyl Butoxide Administered to Mice in the Diet." *Food Additives and Contaminants* 20, no. 3: 207–214. https://doi.org/10.1080/0265203021000050617.

Tanaka, T., and A. Inomata. 2015. "Effects of Maternal Exposure to Piperonyl Butoxide (PBO) on Behavioral Development in F1-Generation

Mice." *Birth Defects Research. Part B, Developmental and Reproductive Toxicology* 104, no. 6: 227–237. https://doi.org/10.1002/bdrb.21163.

Tanaka, T., and A. Inomata. 2016. "Reproductive and Neurobehavioral Effects of Maternal Exposure to Piperonyl Butoxide (PBO) in F1-Generation Mice." *Birth Defects Research. Part B, Developmental and Reproductive Toxicology* 107, no. 4–5: 195–205. https://doi.org/10.1002/bdrb.21185.

Tanaka, T., O. Takahashi, S. Oishi, and A. Ogata. 2009. "Effects of Piperonyl Butoxide on Spontaneous Behavior in F1-Generation Mice." *Toxicology and Industrial Health* 25, no. 7: 489–497. https://doi.org/10.1177/0748233709346756.

Tekendo-Ngongang, C., M. Muenke, and P. Kruszka. 2020. "Holoprosencephaly Overview." In *GeneReviews(R)*, edited by M. Adam, H. Ardinger, R. Pagon, et al. University of Washington.

Wagner, G. C., K. R. Reuhl, M. Cheh, P. McRae, and A. K. Halladay. 2006. "A New Neurobehavioral Model of Autism in Mice: Pre- and Postnatal Exposure to Sodium Valproate." *Journal of Autism and Developmental Disorders* 36, no. 6: 779–793. https://doi.org/10.1007/s10803-006-0117-y.

Wang, J., J. Lu, R. Mook, et al. 2012. "The Insecticide Synergist Piperonyl Butoxide Inhibits Hedgehog Signaling: Assessing Chemical Risks." *Toxicological Sciences* 128, no. 2: 517–523. https://doi.org/10.1093/toxsci/kfs165.

Wang, L.-C., and G. Almazan. 2016. "Role of Sonic Hedgehog Signaling in Oligodendrocyte Differentiation." *Neurochemical Research* 41, no. 12: 3289–3299. https://doi.org/10.1007/s11064-016-2061-3.

Wichterle, H., D. H. Turnbull, S. Nery, G. Fishell, and A. Alvarez-Buylla. 2001. "In Utero Fate Mapping Reveals Distinct Migratory Pathways and Fates of Neurons Born in the Mammalian Basal Forebrain." *Development* 128, no. 19: 3759–3771.

Winkler, C. C., O. R. Yabut, S. P. Fregoso, et al. 2018. "The Dorsal Wave of Neocortical Oligodendrogenesis Begins Embryonically and Requires Multiple Sources of Sonic Hedgehog." *Journal of Neuroscience* 38, no. 23: 5237–5250. https://doi.org/10.1523/JNEUROSCI.3392-17.2018.

Wobbrock, J. O., L. Findlater, D. Gergle, and J. J. Higgins. 2011. "The Aligned Rank Transform for Nonparametric Factorial Analyses Using Only Anova Procedures." *Proceedings of the SIGCHI Conference on Human Factors in Computing Systems*, Vancouver, BC, Canada. https://doi.org/10.1145/1978942.1978963.

Wong, H., B. Alicke, K. A. West, et al. 2011. "Pharmacokinetic-Pharmacodynamic Analysis of Vismodegib in Preclinical Models of Mutational and Ligand-Dependent Hedgehog Pathway Activation." *Clinical Cancer Research* 17, no. 14: 4682–4692. https://doi.org/10.1158/1078-0432.CCR-11-0975.

Wong, H., J. Z. Chen, B. Chou, et al. 2009. "Preclinical Assessment of the Absorption, Distribution, Metabolism and Excretion of GDC-0449 (2-Chloro-N-(4-Chloro-3-(Pyridin-2-Yl)phenyl)-4-(Methylsulfonyl) benzamide), an Orally Bioavailable Systemic Hedgehog Signalling Pathway Inhibitor." *Xenobiotica* 39, no. 11: 850–861. https://doi.org/10.3109/00498250903180289.

Xu, Q., I. Cobos, E. De La Cruz, J. L. Rubenstein, and S. A. Anderson. 2004. "Origins of Cortical Interneuron Subtypes." *Journal of Neuroscience* 24, no. 11: 2612–2622. https://doi.org/10.1523/jneurosci.5667-03.2004.

Zhang, Y., G. Liu, T. Guo, et al. 2020. "Cortical Neural Stem Cell Lineage Progression Is Regulated by Extrinsic Signaling Molecule Sonic Hedgehog." *Cell Reports* 30, no. 13: 4490–4504. https://doi.org/10.1016/j.celrep.2020.03.027.

Supporting Information

Additional supporting information can be found online in the Supporting Information section.